DETERMINATION OF LOCAL TEMPERATURES CAUSED BY ACOUSTIC CAVITATION

Kenneth S. Suslick, Raymond E. Cline, Jr., and David A. Hammerton

School of Chemical Sciences
University of Illinois at Urbana-Champaign
505 S. Mathews Avenue
Urbana, Illinois 61801

Abstract

By the use of comparative rate thermometry, we have been able to determine experimentally the effective temperature created during acoustic cavitation in liquids. The sonochemical reactions of a series of volatile metal carbonyls have been used as chemical dosimeters in alkane solvents. We have established the existence of and conditions present in two reaction sites during acoustic cavitation: a gas phase hot-spot with an effective temperature of 5200K and an enveloping, heated liquid shell with an average effective temperature of ~1900K. A simple conduction model of thermal transport in the liquid reaction site gives qualitative agreement with the chemical dosimetry, and predicts that the liquid reaction zone extends for ~200nm from the surface of the collapsed cavity and has an effective lifetime <2usec.

1. Introduction

The chemical effects of ultrasound have been studied for fifty years [1], and recent interest in this area, in fact, has been intense [2,3,4,5,6]. In spite of this, a detailed understanding of the reaction conditions created by ultrasonic irradiation of liquids has not been available. It is well established [7,8,9] that localized, short-lived "hot-spots" created by ultrasonic cavitation are the origin of such sonochemistry, and early theoretical calculations using hydrodynamic models of cavitational collapse gave temperature and pressure estimates of 10,000K and 10,000 atmospheres [10]. More recent studies have estimated the temperatures and pressures to be 2000K and 1000 atmospheres [11,12], but because of assumptions made with respect to thermal transport, vapor concentration, etc., these models are difficult to use in a predictive fashion.

Prior experimental determination of the conditions generated during cavitational collapse is sparse and is based exclusively on sonoluminescence in aqueous solutions. Verrall and Sehgal have studied sonoluminescence of aqueous solutions saturated with alkali metal salts [13] and with NO and NO_2 gases [14]. From data obtained in these experiments, they estimated cavitational temperatures to be 860K for NO_2 saturated solutions, 1350K for NO saturated solutions, and 3400K for alkali metal salt solutions. These experiments, however, may not be probing the cavitation event, since sonoluminescence is caused by radical recombination which may or may not occur directly in the hot spot. For example, sonoluminescence from excited Na atoms cannot be occurring in the gas-phase of the collapsing bubble, because they are produced by reduction of Na^+ which has no volatility. Another recent study made use of aqueous sonoluminescence as a function of ambient temperature in order to estimate temperatures generated during cavitation [15]. In addition to the earlier point concerning the site of luminescence, this estimation relies on a complex kinetic model.

Using the ligand substitution rates of volatile metal carbonyls as dosimeters, we have been able to establish the site of sonochemical reactions [16,17]. We find that there are two regions of sonochemical reactivity: one corresponding to the gas phase within the collapsing cavity and the second to a thin liquid layer immediately surrounding the collapsing cavity. Furthermore, we have been able to determine experimentally, using comparative rate thermometry, the effective temperature distribution in each reaction zone.

2. Experimental Details

All ultrasonic irradiations were made with a collimated (far field region) 20 kHz beam from a titanium amplifying horn driven by a lead zirconate titanate transducer (Heat Systems Inc.; Model W-375), with a total acoustic absorbed power of 24 W, as determined calorimetrically, and acoustic intensities of 24 W/cm^2 at the surface of the horn. The detailed experimental configuration is described elsewhere [6,18,19].

Solvents were of the highest available purity (spectrophotometric, gold label, or 99%+) and were used without further purification. $Fe(CO)_5$ (from Alpha Ventron Chemicals) was vacuum distilled immediately prior to use. $Cr(CO)_6$, $Mo(CO)_6$, and $W(CO)_6$ (from Alpha Ventron Chemicals) were 95%+ pure and were sublimed before use. $P(C_6H_5)_3$ (from Aldrich Chemical) was 99% pure and was used as

0090-5607/85/0000-1116 $1.00 © 1985 IEEE

purchased. $P(OCH_3)_3$ and $P(OC_6H_5)_3$ (from Aldrich Chemicals) were vacuum distilled before use. Vapor pressures were calculated from available data [20,21,22,23] assuming ideal behavior.

Alkane solutions with metal carbonyl concentrations of 0.01M were irradiated with ultrasound. The alkane solutions were made from mixtures of two alkanes (heptane through dodecane) chosen in the proper proportion to give a total system vapor pressure of 5.0 torr at the chosen bulk temperature (which was varied between 270K and 350K). Reactions were performed in a thermostated amber glass sonication cell, which was kept under a slight positive pressure of argon. Solutions were sparged with argon, then transferred to the sonication cell. Aliquots of the solutions were removed at regular intervals during sonication, and the absorbance of the metal carbonyl was determined using Fourier transform infrared spectrophotometry (Nicolet 7199 or MX-S). First order rate constants were then determined from the plots of log(Absorbance) versus time for each reaction at each chosen, bulk temperature. The bulk temperature was then varied (as were the alkane mixtures to keep the total vapor pressure constant) in order to determine observed sonochemical rates as a function of metal carbonyl vapor pressure. Linear regression analyses were used for quantitative determinations.

Calculations of temperature evolution models were done numerically using an explicit method of finite differencing [24]. The temperature profiles as a function of radial distance and time used the appropriate thermal diffusities for Ar at elevated temperatures for the gas phase reaction zone [24] and for decane in the liquid reaction zone [25]. Initial temperatures in the gas phase reaction zone were set to 5200K, as determined experimentally (and discussed below). The size of the heated sphere was taken at 1.544×10^{-4}m, which is derived from the maximum cavity radius before collapse (6.50×10^{-4}m) and the compression ratio required to generate the observed gas phase temperature [16,17]. Convergence of the solutions were demonstrated by incremental decreases in the step sizes of radial distance and time. Theoretical relative rates in the liquid phase were calculated by trapezoidal integration.

3. Results and Discussion

For this study, we have used four metal carbonyls as dosimeters, $Fe(CO)_5$, $Cr(CO)_6$, $Mo(CO)_6$ and $W(CO)_6$, whose general structures are shown in Fig. 1. We have previously explored the sonochemistry and sonocatalysis of the metal carbonyls in some detail [5,6,18]. Their present use as chemical dosimeters for acoustic cavitation has been successful for several reasons. First, their thermal and photochemical behaviors are well defined and serve as an essential background [26,27] for understanding their sonochemical reactivity. Second, their reactivity is essentially simple, since the carbon-oxygen bond strength is very much larger than the metal-carbon (i.e. >900 KJ/mole difference in bond enthalpies). Third, these reactions are unimolecular in their rate determining step and are not due to secondary reaction in the bulk solution. Fourth, these reactions are easily monitored quantitatively by infrared spectrophotometry. Finally, the kinetic behavior of these systems is extremely well behaved throughout the course of the reactions.

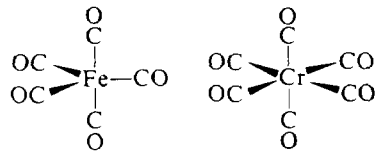

Figure 1. The Structures of Metal Carbonyls.

We have found that the substitution kinetics of these metal carbonyls with various phosphines (PR_3) and phosphites ($P(OR)_3$) are first order in metal carbonyl and zero order in ligand [6]. An example of a kinetic plot of a substitution reaction is shown in Fig. 2. The concentration of

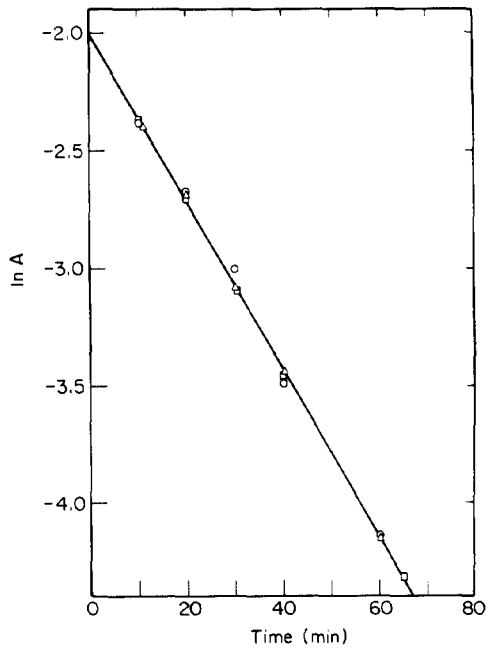

Figure 2. First Order Kinetics of $Fe(CO)_5$ Sonochemical Ligand Substitution with $P(OCH_3)_3$.

$P(OCH_3)_3$ was varied up to a 30-fold excess and no change was seen in the observed rate. This behavior is typical of a dissociative mechanism (see Scheme I, below). Under sonolysis, metal carbon-

Scheme I

$$M(CO)_n \xrightarrow{)))} M(CO)_{n-x} + xCO$$

$$M(CO)_{n-x} + L \longrightarrow M(CO)_{n-x}L$$

$$M(CO)_{n-x} + CO \longrightarrow M(CO)_{n-x} + 1$$

yls may exhibit multiple CO loss. The reactive fragment so formed can then add a ligand, which may be CO or L (L = phosphine or phosphite). If the resulting complex is still coordinatively unsaturated, the fragment will add a second ligand. Products of these reactions are primarily mono- and disubstituted metal carbonyl phosphine (or phosphite) complexes.

As described in the experimental section, the total vapor pressure was kept constant. This is essential since the efficacy of cavitational collapse and the temperatures so generated are strongly dependent on the vapor pressure of the solvent system [28,29]. Therefore, we keep the dosimeter's concentration in the bulk solution constant, fix the total system vapor pressure, and vary the bulk temperature. In this way, we can vary the dosimeter's vapor pressure alone, while keeping all other relevant parameters constant.

This has been done for all four of our dosimeters; Figures 3 and 4 show the results for $Fe(CO)_5$ and $W(CO)_6$, respectively. In all cases, the observed sonochemical rate increases with increasing dosimeter vapor pressure and a has non-zero intercept. The linear dependence of the observed rate coefficients on dosimeter vapor pressure is due to reactions occurring in the gas phase. As the dosimeter vapor pressure increases, its concentration within the gas phase cavity increases linearly, thus increasing the observed sonochemical rate coefficients. The non-zero intercept indicates that there is a vapor pressure independent component of the overall rate. That is, there must be an additional reaction site occurring within the liquid phase. Because one would expect localized heating of the liquid near the collapsing cavity, we believe the liquid phase reaction is occurring in the thin liquid shell surrounding the collapsing cavity, as illustrated in Fig. 5. These results demonstrate that there

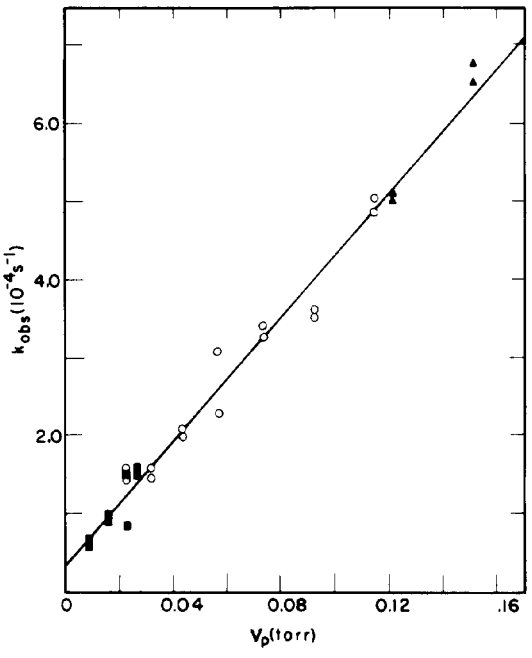

Figure 3. Observed First-Order Sonochemical Rate Coefficients for $Fe(CO)_5$ vs. the Vapor Pressure of $Fe(CO)_5$. The total vapor pressure of the system is constant at 5.0 torr.

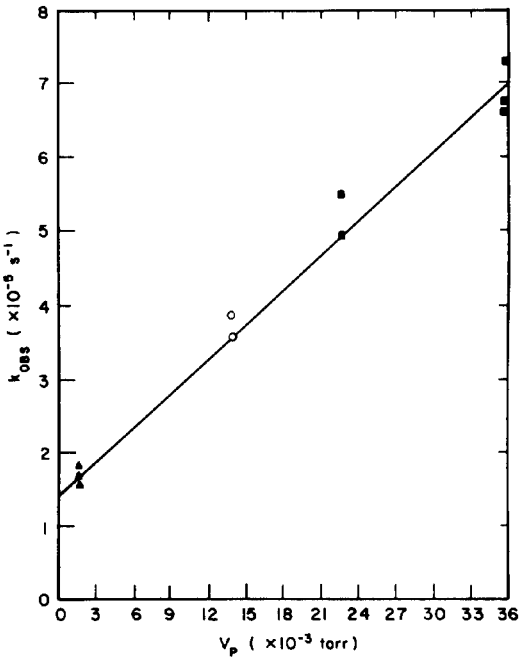

Figure 4. Observed First-Order Sonochemical Rate Coefficients for $W(CO)_6$ vs. the Vapor Pressure of $W(CO)_6$. The total vapor pressure of the system is constant at 5.0 torr.

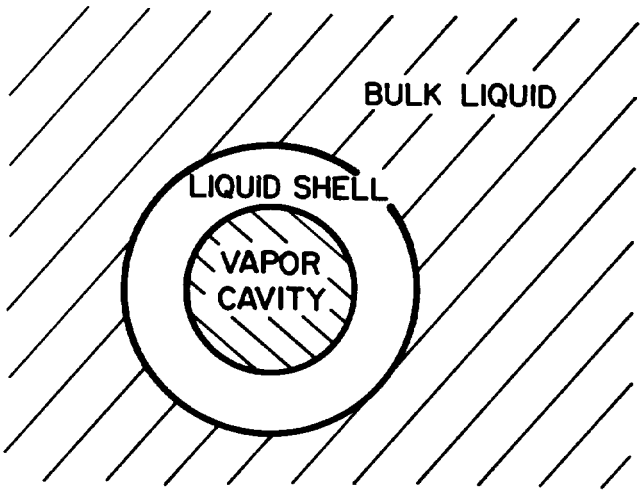

Figure 5. Two Site Model of Sonochemical Reactivity.

are two sonochemical reaction zones: a gas phase site and a liquid phase site.

We can further analyze our data to estimate the effective temperatures reached in each site by the use of comparative rate thermometry, a technique developed for similar use in shock tube chemistry [30]. If one has a series of reactions whose rate behavior as a function of temperature is known, then from their experimentally determined relative rates one may calculate the effective temperature at which the reactions occurred. For the dissociation of CO from a series of metal carbonyls, the Arrhenius parameters {k = $Aexp(-E_a/RT)$, where k = rate coefficient, A = activation frequency, E_a = activation energy, R = gas constant} have recently been accurately determined at high temperatures by gas phase laser pyrolysis [31].

From the slopes and intercepts of Figures 3 and 4 (and similar plots for the other complexes), we can derive the rate coefficients (shown in Table I) for the gas phase and liquid phase reaction sites [17]. The effective temperature of each

Table I.

Dosimeter	$k_g(sec^{-1}bar^{-1})^a$	$k_\ell(sec^{-1}M^{-1})$
$Fe(CO)_5$	2.96(5)	$3.35(48) \times 10^{-3}$
$Cr(CO)_6$	2.45(72)	$12.2(10) \times 10^{-3}$
$Mo(CO)_6$	1.63(14)	$2.97(25) \times 10^{-3}$
$W(CO)_6$	1.17(6)	$1.37(18) \times 10^{-3}$

[a] k_g is the gas phase reaction constant (taken from the slopes of the lines fit to data in Figures 3 and 4, etc); k_ℓ is the liquid phase reaction rate constant (taken from the intercepts of the data in Figure 3 and 4, etc.).

[b] The standard deviation of last digit is given in parentheses.

site can be calculated from the slope of plots of $\log(A/k_{obs})$ versus E_a for our four dosimeters. Figure 6 shows such a plot for the gas phase reaction site. The data are quite good for the gas phase reaction zone, and give an estimate of the gas phase effective temperature of 5200 ± 650K, under our conditions.

The liquid phase zone does not behave as well, as shown in Figure 7: this is expected, since there must be a spatial temperature gradient in the liquid surrounding the gas phase hot-spot, rather than a single, uniform temperature. A more realistic view of the temperature and rate profile in the liquid reaction zone is shown in Figure 8. We have modelled the time and spatial evolution of the liquid zone temperature using an explicit method of finite differencing, as described earlier, based on a sphere at initial temperature of 5200K embedded in an infinite matrix at 300K. This is an admittedly simple model which includes only

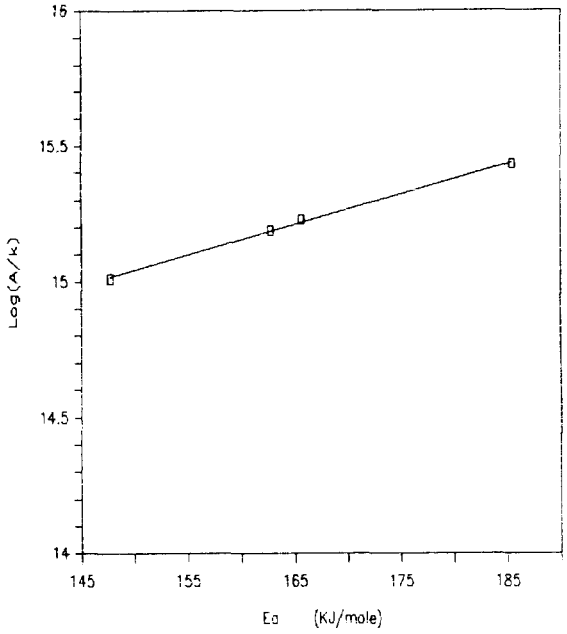

Figure 6. Comparative Rate Thermometry of the Gas Phase Reaction Site. In order of increasing E_a, these data are for $Cr(CO)_6$, $Mo(CO)_6$, $Fe(CO)_5$, and $W(CO)_6$. The slope of the least squares fit line (solid) is $1/RT_{eff}$.

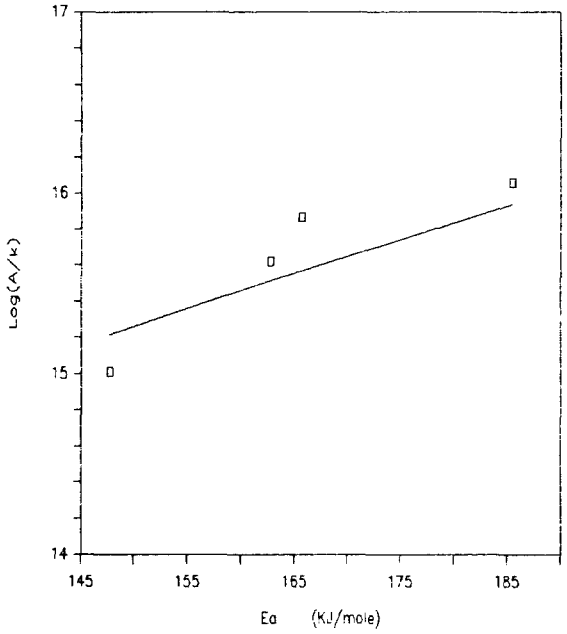

Figure 7. Comparative Rate Thermometry of the Liquid Phase Reaction Site. In order of increasing E_a, these data are for $Cr(CO)_6$, $Mo(CO)_6$, $Fe(CO)_5$ and $W(CO)_6$. The solid line in this case is derived from the conduction model of thermal transport described in text.

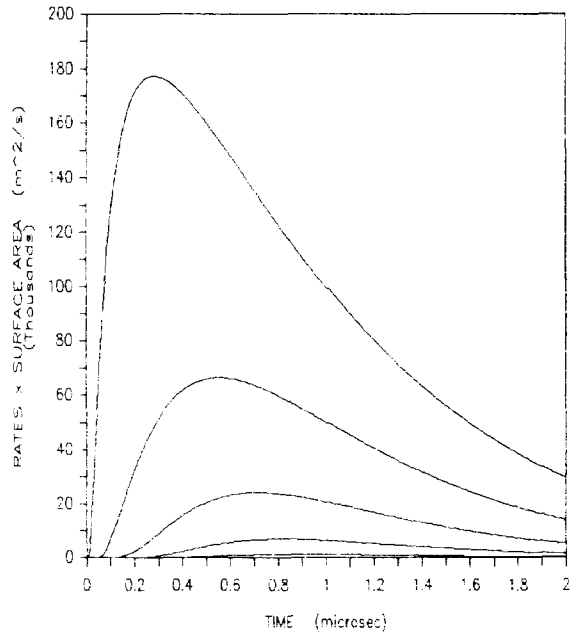

Figure 8. Calculated Reaction Rates in the Liquid Phase Reaction Site as a Function of Time and Distance from Bubble Surface. These rates for $W(CO)_6$ were derived from the conduction model described in text, and weighted by annular volume. In descending order, the distances from the bubble surface are 50, 100, 150, 200, and 250nm.

conductive heat transport; convection is not included. It should be emphasized that our simple conduction model has no adjustable parameters in predicting relative rates. Remarkably, this model does agree qualitatively with the data. Using the activation parameters (E_a and A) derived from gas phase pyrolysis, our model predicts the relative liquid phase rates to be in the same order actually observed: $Cr(CO)_6$ > $Fe(CO)_5$ > $Mo(CO)_6$ > $W(CO)_6$, which is different than those of the gas phase site. As shown in Figure 7, our simple heat conduction model predicts relative rates which are in rough agreement with the observed liquid phase reaction zone.

The quantitative comparisons are only fair, however: relative rates for $W(CO)_6$, $Mo(CO)_6$, $Fe(CO)_5$ and $Cr(CO)_6$ are, 1.00, 2.16, 2.44 and 8.89 as observed, and 1.00, 2.11, 3.70, and 4.21 as calculated from our model. The model predicts a spatial and temporal average liquid zone reaction temperature of 2730K; the experimentally determined data give a liquid zone temperature of ~1900K. Convection and mass transport effects would lower the temperatures predicted in the liquid reaction zone, and would bring the model into better quantitative agreement and the observed data.

The conduction model also gives us a sense of scale concerning the liquid reaction zone: it extends only ~200nm from the bubble surface, and it has an effective lifetime of less than 2 μsec after collapse. The size of this heated shell corresponds to a reactive liquid layer of ~500 molecules thick.

Another way to estimate the depth of this liquid zone is to assume complete reaction of all metal carbonyl molecules in both the gas phase and liquid phase zones. With that assumption, the ratio of k_ℓ to k_g easily gives the approximate ratio of volumes (and radii) of the liquid to gas zones immediately before collapse [16]. With our data, the gas phase to liquid phase reaction site volumes are ~1.5×10^4 before collapse. If we estimate our bubble radius before collapse as 6.5×10^{-4}m [16,32], then in order to generate a final temperature of 5200K, the bubble radium after collapse will be ~1.5×10^{-4}m. This leads to an estimate of the liquid reaction zone depth of 270nm, which is in good agreement with our simple conduction model.

4. Acknowledgements

We thank Dr. H. H. Wang for his efforts early in this study and Professor Michael M. Chen for his helpful discussions on heat transfer theory. This work has been supported by the N.S.F. (Chemical Dynamics, CHE 8319929). A Sloan Foundation Research Fellowship (K.S.S.) and a N.I.H. Research Career Development Award (K.S.S.) are gratefully acknowledged.

[1] I. E. Elpiner Ultrasound: Physical, Chemical, and Biological Effects. New York: Consultants Bureau, 1964.

[2] K. S. Suslick "Organometallic Sonochemistry" Adv. Organomet. Chem., vol. 25, 1986.

[3] J. L. Luche "Some aspects of organic acoustochemistry" Actual. Chim., issue 8, pp. 21-6, 1982.

[4] P. Boudjouk "Organic chemistry with ultrasound" Nachr. Chem., Tech. Lab., vol. 31, pp. 798-800, 1983.

[5] K. S. Suslick and R. E. Johnson "Ultrasonic Activation of Early Transition Metals" J. Am. Chem. Soc., vol. 106, pp. 6856-8, 1984.

[6] K. S. Suslick, J. W. Goodale, H. H. Wang, and P. F. Schubert "Sonochemistry and Sonocatalysis of Metal Carbonyls" J. Am. Chem. Soc., vol. 105, pp. 5781-5785, 1983.

[7] M. E. Fitzgerald, V. Griffing, and J. Sullivan "Chemical Effects of Ultrasonics -'Hot-Spot' Chemistry" J. Chem. Phys., vol. 25, pp. 926-933, 1956.

[8] M. A. Margulis "Electrical Phenomena Associated with Cavitation" Russ. J. Phys. Chem., vol. 55, pp. 81-85, 1981.

[9] C. M. Sehgal and R. E. Verrall "Review of the Electrical Hypothesis of Sonoluminescence" Ultrasonics, vol. 20, pp. 37-39, 1982.

[10] Lord Rayleigh, Phil. Mag, Ser. 6, vol. 34, pp. 94-98, 1917.

[11] M. A. Margulis and A. F. Dmitrieva "Dynamics of Cavitation Bubble Collapse" Zh. Fiz. Khim., vol. 56, pp. 323-327, 1982.

[12] S. Fujikawa and T. Akamatsu "Effects of the Non-equilibrium Condensation of Vapour on the Pressure Wave Produced by the Collapse of a Bubble in a Liquid" J. Fluid Mech., vol. 97, pp. 481-521, 1980.

[13] C. Sehgal, R. P. Steer, R. G. Sutherland, and R. E. Verrall "Sonoluminescence of Argon Saturated Alkali Metal Salt Solution as a Probe of Acoustic Cavitation" J. Chem. Phys., vol. 70, pp. 2242-2248, 1979.

[14] C. Sehgal, R. G. Sutherland, and R. E. Verrall "Sonoluminescence of NO and NO_2 Saturated Water as a Probe of Acoustic Cavitation" J. Phys. Chem., vol. 84, pp. 396-401, 1980.

[15] P. K. Chendke and H. S. Fogler "Variation of Sonoluminescence Intensity of Water with Liquid Temperature" J. Phys. Chem., vol. 89, pp. 1673-1677, 1985.

[16] K. S. Suslick and D. A. Hammerton "The Site of Sonochemical Reactions" I.E.E.E. Son. Ultrason. Trans., 1986, in press.

[17] K. S. Suslick and D. A. Hammerton "The Site and Nature of Sonochemical Reactions" Ultrasonics Intl. Symposium Proceedings, 1985, in press.

[18] K. S. Suslick and P. F. Schubert "Sonochemistry of $Mn_2(CO)_{10}$ and $Re_2(CO)_{10}$" J. Am. Chem. Soc., vol. 105, pp. 6042-6044, 1983.

[19] K. S. Suslick, P. F. Schubert, and J. W. Goodale "Chemical Dosimetry of Ultrasonic Cavitation" IEEE Ultrasonics Symposium Proceedings, vol. 1, pp. 612-616, 1981.

[20] J. A. Riddick and W. G. Bunger Techniques of Chemistry: Organic Solvents; Wiley-Interscience: New York, 1970; vol. 2.

[21] A. G. Dilbert and K.G.P. Sulzmann "The Vapor Pressure of Iron Pentacarbonyl" J. Electrochem. Soc., vol. 121, pp. 832-834, 1974.

[22] F. A. Cotton and R. R. Monchamp "The Heat of Sublimation and the Metal-Metal Bond Energy in $Mn_2(CO)_{10}$" J. Chem. Soc., pp. 533-536, 1960.

[23] L. Fabbrizzi, R. Mascherini, and P. Paoletti "Melting of Group VI Transition Metal Hexacarbonyls: Thermodynamics Parameters" J. Chem. Soc., Faraday Trans. I, vol. 72, pp. 896-900, 1976.

[24] M. N. Özişik Basic Heat Transfer. New York: McGraw-Hill, 1977.

[25] Y. Touloukian, P. Liley, and S. Saxena, Eds. Thermophysical Properties of Matter, vol 3., Thermal Conductivity, Nonmetallic Liquids and Gases, New York: IFI/Plenum, 1970.

[26] G. Wilkinson, F.G.A. Stone, and E. W. Abel, Eds. Comprehensive Organometallic Chemistry: The Synthesis, Reactions and Structures of Organometallic Compounds New York: Pergamon Press, 1982; vols. 3, 4, 5, 6, 8.

[27] G. L. Geoffroy and M. S. Wrighton Organometallic Photochemistry; New York: Academic Press, 1979.

[28] K. S. Suslick, J. W. Gawienowski, P. F. Schubert, H. H. Wang "Alkane Sonochemistry" J. Phys. Chem., vol. 87, pp. 2299-2301, 1983.

[29] K. S. Suslick, J. W. Gawienowski, P. F. Schubert, H. H. Wang "Sonochemistry in Non-Aqueous Liquids" Ultrasonics, vol. 22, pp. 33-36, 1984.

[30] W. Tsang "Comparative-Rate Single-Pulse Shock Tube Studies", A. Lifshitz, Ed. Shock Waves in Chemistry, New York: Marcel Dekker, 1981, pp. 59-182.

[31] N. F. Lewis, D. M. Golden, and G. P. Smith "Organometallic Bond Dissociation Energies: Laser Pyrolysis of $Fe(CO)_5$, $Cr(CO)_6$, $Mo(CO)_6$, and $W(CO)_6$" J. Am. Chem. Soc., vol. 106, pp. 3905-3912, 1984.

[32] R. E. Apfel "Acoustic Cavitation" in Ultrasonics, P. D. Edmonds, Ed. New York: Academic Press, 1981, pp. 356-413.